Journal of the European Ceramic Society 15 (1995) 469–477
Elsevier Science Limited
Printed in Great Britain.
0955-2219/95/$9.50

0955-2219(95)00009-7

Compaction and Sintering Behaviour of Sol–Gel Powders

Y. Jorand,[a] M. Taha,[a] J. M. Missiaen,[b,d] & L. Montanaro[c]

[a]G.E.M.P.P.M., U.R.A. C.N.R.S. 341, I.N.S.A. Lyon, Bat. 502, 69621 Villeurbanne Cedex, France
[b]C.P.P.I., E.N.S. des Mines de Saint-Etienne, 158 cours Fauriel, 42100 Saint-Etienne, France
[c]Department Materials Science & Chemical Engineering, Politecnico, Corso Duca degli Abruzzi 24, 10129 Torino, Italy.
(Received 4 December 1992; revised version received 11 September 1994; accepted 12 December 1994)

Abstract

Dry pressing is the most common industrial shaping process for ceramic pieces. Sol–gel powders are of high reactivity, but very often agglomeration–aggregation phenomena limit this advantage by inducing poor compaction behaviour. Consequently the goal of sol–gel powder research — to obtain full densification at very low sintering temperature, is not achieved. With the intention of showing the influence of sol–gel powders, specific characteristics on pressing, compaction diagrams and green body characteristics of two experimental zirconia sol–gel powders have been determined. For comparison a well-known commercial product was used as a control. These observations were correlated as densification tests and initial powder characteristics. The sol–gel powder parameters that must be adapted to dry pressing forming and the incidence of the synthesis conditions, have emerged.

1 Introduction

Dry pressing is a method extensively used for the industrial production of ceramics. It is well known that the quality of ceramic bodies is strongly influenced by the characteristics of the starting powder. A powder having good compaction behaviour gives a high-density green compact and, more importantly, a fine and homogenous porosity. This results in a high-density sintered body as already shown in many studies.[1]

The major source of the defects observed in a green body originates in the characteristics of the different constituents of the powder. The different constituents of a powder can be defined in different ways, so we will explain the definitions used in this text. The smallest unit of a powder which can be considered is the crystallite. It can be defined as a coherently diffracting region, and measured by X-ray diffraction line broadening. In a first approximation, the potential reactivity of a powder can be linked to the crystallite size (in fact a crystal can be constituted of several crystallites): this is not far away from the minimal particle size that can be individualised. In classical powder processing these particles do not appear alone, but clustered into either the aggregates or the agglomerates, depending upon the nature of the binding forces. An aggregate is an arrangement of crystallites held together by strong binding forces, e.g. chemical bands in solid bridges. A typical example is the aggregates formed during calcination of Bayer aluminas. Consequently, aggregates retain their identity under a wide variety of severe conditions, and especially under high compaction pressure.[2] The agglomerates are constituted of crystallites and/or aggregates held by weak binding forces, such as Van der Walls or electrostatic forces. Agglomerates, in contrast to aggregates, are much more easily disrupted by external forces.

All fine particle size ceramic powders contain agglomerates, because Van der Walls forces exceed gravitational ones, and very often, depending on the synthesis process, aggregates. When the powder is poured into a compaction die, one can distinguish three porosity types: interagglomerate, interaggregate and intraaggregate porosities. Irregularly shaped particles (agglomerates and/or aggregates) affect the flowability of the powder, and lead to the creation of gross interagglomerates/interaggregate porosities by promotion of arch formations. If agglomerates, or more frequently aggregates, are resistant to compaction forces, this induces packing inhomogeneities in the green

[d]Now at: Laboratoire de Thermodynamique et Physico-Chimie Métallurgiques, E.N.S.E.E.G., B.P. 75, 38402 St Martin D'Hêre Cedex, France.

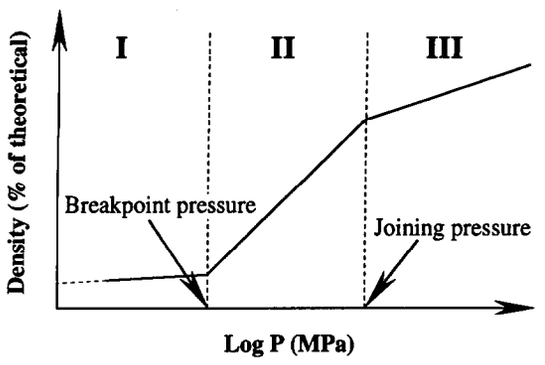

Fig. 1. Typical compaction response diagram for granulated or agglomerated powders.

body associated to important interagglomerates/ interaggregate porosities. During sintering, the denser regions formed by remaining agglomerates/ aggregates will first densify at low temperatures, then the interagglomerates/interaggregate porosities will grow, or more detrimentally, transform into cracklike defects: these porosities will require for their elimination, if it ever happens high temperatures and long sintering times.[3-4]

In classical powder metallurgy processes, the powders are granulated after deagglomeration/ aggregation treatments in order to avoid the problems mentioned earlier. An ideal granulate should be: spherical with the smallest diameter possible while enough to allow good flowability, dense and resistant to industrial manipulations, but plastically deformed under low compaction pressures to fill the intergranulate voids.

Compaction tests are useful tools for characterising the powder pressing operation. Various testing methods have been developed:[5] the most extensively reported is the compaction response diagram that relates the relative density of the compact to the logarithm of the compaction pressure. These tests are quite sensitive to the strength variations of the different particles contained in a powder, and gives good information on the compaction behaviour.[6] The typical compaction response diagram of granulated (or agglomerated) powder is given in Fig. 1. This compaction behaviour has been explained by many authors,[5,7,8] and is summarised below. The curve can be divided into three linear portions. At low pressure the density remains relatively constant which corresponds to granulate rearrangement. The limit between the two first parts defines the breakpoint pressure which is a measurement of granulate (or agglomerate) strength. The second linear portion corresponds to the rearrangements provoked during and after the crushing or deformation of the granulates. The slope remains constant up to a joining pressure where the granules (or the agglomerates) lose their separate identity. Then in the third linear part, the compact behaviour is similar to the same nongranulated (agglomerated) powder. This corresponds to the rearrangement of the crystallites (or aggregates if any). Aggregates, in the sense of the definition given here, cannot be broken under the pressure usually used for compaction tests. Indeed, for example, aggregates formed by calcination in Bayer aluminas require pressures up to 700 MPa to be broken.[8] It can be assumed that the same sequence as for agglomerates is repeated since the aggregates are fractured.

The quality of sintered bodies is also dependent on the physico-chemical characteristics of the powder: the sol–gel methods allow the synthesis of powders having high homogeneity, purity, and reactivity.[9] Sol–gel powders can exhibit crystallite clusters that can be related to granulates in the sense that their morphology and diameters are well controlled. But very often the crystallites contained in these clusters are strongly bonded.[10] This limits their compaction behaviour and does not permit them to benefit from their high reactivity. These pseudo-granules are defined as granules in this paper.

This work compares the compaction and sintering of two sol–gel powders to that of a commercial powder. It is expected that this kind of measurement will give feed-back on how to improve the synthesis process of these powders.

2 Experimental Procedure

Three powders have been studied. The control, labelled P1, is a commercial well-known powder of ZrO_2 + 3 mol% Y_2O_3 (5·8 mol% Y in ZrO_2), TOSOH TZ-3YB. P2 and P3 are ZrO_2 experimental powders. P2 contains 3·6 mol% Y_2O_3 (6·9 mol% Y in ZrO_2). This powder was prepared by a sol–gel technique using monomeric solutions of mixed inorganic salts modified by the addition of high viscosity organic polymers. The resulting viscous solution was sprayed in ammonium hydroxide to form gel particles of mixed hydroxides that were dehydrated by azeotropic distillation. After that the powder was heat-treated at 700°C for 4 h. P3 composition was synthesised with 2 mol% Y_2O_3 (3·9 mol% Y in ZrO_2) by gel coprecipitation starting from inorganic salt solutions[11] $ZrCl_4$ and YCl_3–7 H_2O. The gel obtained was first washed in water, then in ethyl alcohol. The alcohol washing was performed to avoid hard agglomeration occurrence, which derived from the hydroxy-bridges produced by the presence of water on the micelles surface. The alcoholic colloidal suspension obtained was oven-dried at 80°C. Then the resulting agglomerated powder was passed through a 40

μm sieve. This powder was heat-treated at 600°C for 30 min. This calcination temperature was chosen to ensure a development of crystalline phase without a strong decrease of specific surface area.

The powders have been characterised by means of scanning electron microscope (SEM), laser granulometry, BET adsorption method and X-ray diffraction analysis in order to determine the nature and amount of different phases and the crystallite size. The phase (monoclinic and tetragonal ZrO_2) percent composition was evaluated using the relationship presented in Ref. 12 The crystallite size was calculated with the Scherrer formula, after correcting the experimental effect by a parabolic law.[13]

The compaction tests were performed on an INSTRON mechanical testing machine, in the range 0–200 MPa with a crosshead rate of 0·5 mm/min. 2 g powder samples were poured into a cylindrical die of a 10 mm diameter, then the tap density was achieved[14] before conducting the compaction test. The density variation during pressing was deduced from the crosshead continuous displacement. Deviation due to the elastic compliance of the load cell was nullified carrying out a blank test, using the same units of measurement without powder in the die and recording its response in the same pressure range. These compaction tests allowed us to draw the relationship between density and compaction rate versus applied pressure. The tap density is approximated by measuring the density at the early stage of pressing, i.e. at sufficiently low pressure.

Hg porosimetric measurements were carried out on 0·5 g powder samples, uniaxially pressed at 100, 200, and 400 MPa, in order to follow the evolution of pore size distribution during compaction. The data were used to draw the variation of relative and cumulative pore volume as a function of pore radius.

Sintering was studied by dilatometric measurements performed on 2 g pellets obtained by 50 MPa uniaxial pressing, followed by 400 MPa isostatic pressing. Heating rate of 1°C/min and a final temperature of 1500°C were chosen. In addition, pellets were sintered, with the same pressing conditions and heating rate, up to 1350°C and 1500°C respectively, and maintained at these temperatures for 2 h. These samples were characterised by SEM observations and X-ray diffraction analysis, in order to define the nature and amount of phases, using the same protocol as for the starting powders. Hg porosimetry and He pycnometry were also conducted, in order to quantify the open and close porosity respectively, and therefore the apparent density.

Table 1. Powder characteristics

Powder	*Granulate size distribution (μm)*			*Phase composition (%)*	*Mean crystallite size (nm)*	*Specific surface area BET (m^2/g)*
	D_{50}	D_{10}	D_{90}			
P1	53·5	18	84	100% tetra	93	17
P2	34	10	52	100% tetra	9	100
P3	12·5	2·8	37·5	100% tetra	9	80

D_{50}: 50% of the distribution with equivalent diameter below D_{50}.
D_{10}: 10% of the distribution with equivalent diameter below D_{10}.
D_{90}: 90% of the distribution with equivalent diameter below D_{90}.

3 Results and Discussion

The physico-chemical characteristics of the powders are summarised in Table 1. All the powders contained spheroidal granules. But SEM observations show that the P1 powder is constituted of hollow granules characteristic of a spray-drying process. When compared to P1, the P2 and especially P3 granules are finer. It can be seen from Table 1 that the granule size distribution of P3 powder is broader than P1 and P2: the D_{50}/D_{10} and the D_{90}/D_{50} ratios are respectively 3 and 4·5 for P3 and about 1·5 and 3–3·4 for P1 and P2.

The main differences between the three powders are the crystallite size and the specific surface area: both sol–gel powders (P2 and P3) exhibit a smaller crystallite size and a higher specific surface area than the P1 powder. The values obtained are usual for sol–gel powders heat-treated at low temperature (600 and 700°C), because, under these conditions, grain coarsening is negligible.

A relative tap density of 20% is obtained for the P1 powder, while lower values, between 10 and 15%, are obtained with the sol–gel powders. It is well known that tap density is strongly dependent on particle size: with fine powders, the Van der Waals forces between particles are much higher than gravitational forces and this affects the flowability[15] (this is why granulation is required with fine powders). For zirconia it has been calculated that the particulate size limit required for these two forces to be equal is about 20 μm diameter.[16] This means that granulation is efficient for the P1 powder, because it contains a low amount of fine granules with diameter less than this limit (D_{10} value is 18 μm). But in the case of the P2 and P3 powders, the granules are too small, D_{10} values are of 10 and 2·8 μm respectively. A bad filling of the compaction dies is therefore obtained, resulting in low tap densities. These observations were made while P1 contained hollow granules which can reasonably be supposed to be the less dense. Consequently it can be assumed that low flowability due to the P2 and P3 granule sizes when compared to P1 as a predominant effect than granule densities.

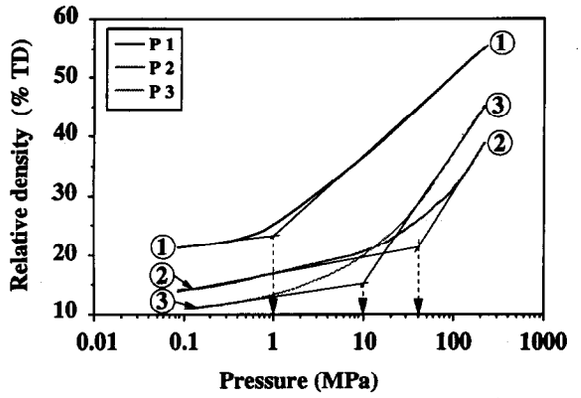

Fig. 2. Compaction response diagram of P1, P2 and P3 powders.

The relative green density (% TD) versus the applied pressure (P) curves (Fig. 2) demonstrate the better compaction behaviour of powder P1: its green density reaches about 50% TD for a pressure of 100 MPa, while 31% TD and 38% TD are reached for P2 and P3 powders. The breakpoint pressure is about 1 MPa, 40 MPa and 10 MPa for P1, P2 and P3 respectively. The compaction rate diagrams (Fig. 3) show that the compaction rate for P1 increases rapidly until 1·5 MPa, and then become stable. This plateau was also observed for the P3 powder, but only starting from 50 MPa. It was not observed for the P2 powder in the range of investigated pressures. It can be assumed that when the maximum compaction rate is obtained, the crushing or deforming of all the granulates is achieved, because they all have successively been submitted to their maximum strength by the net forces developed in the powder arrangement. So the constant compaction rate observed must correspond to reorganisation of the particles provided by the crushed or deformed granulates.

Figure 4 gives the pore size distributions of powders uniaxially pressed at 100, 200, and 400 MPa. A pressure of 100 MPa induces in the P1 sample a monomodal pore distribution of mean radius equal to 16–20 nm. This can be attributed

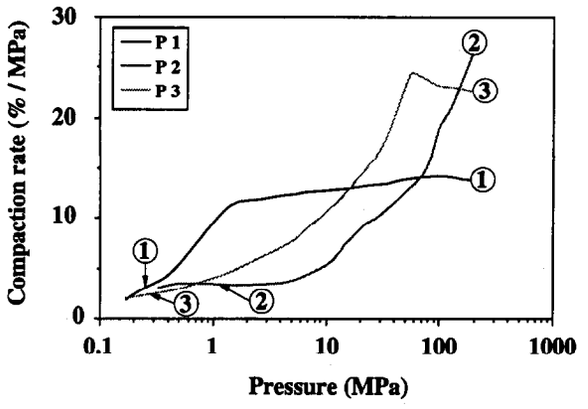

Fig. 3. Compaction rate diagram of P1, P2 and P3 powders.

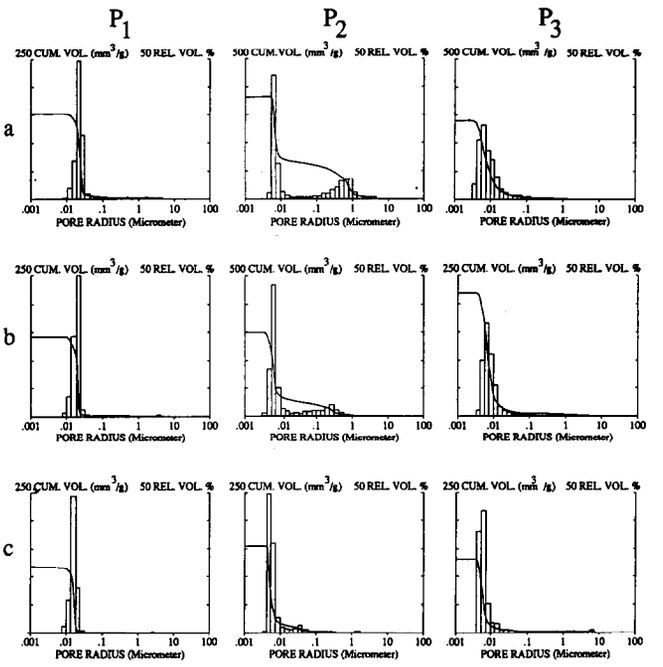

Fig. 4. Pore size distribution for P1, P2 and P3 powders pressed at: (a) 100 MPa, (b) 200 MPa and (c) 400 MPa.

to the fact that only intercrystallite pores (crystallite mean diameter of 93 nm) subsist, since reorganisation of particles due to compaction is still well progressed at this pressure. The pore distribution of the P3 sample pressed at 100 MPa is also monomodal but broader, ranging between 4 and 100 nm. This corresponds to intercrystallite pores that have still not been reduced by particle reorganisation. An increase of the pressure leads to a narrower distribution by reducing the larger intercrystallite pores that are less stable. Consequently higher pressure is required to reach the same green state as the P1 compacts. The porosity evolution of the P2 sample is more complex. At 100 MPa, it shows a bimodal distribution with the maxima at 7 and 800 nm, which correspond respectively to

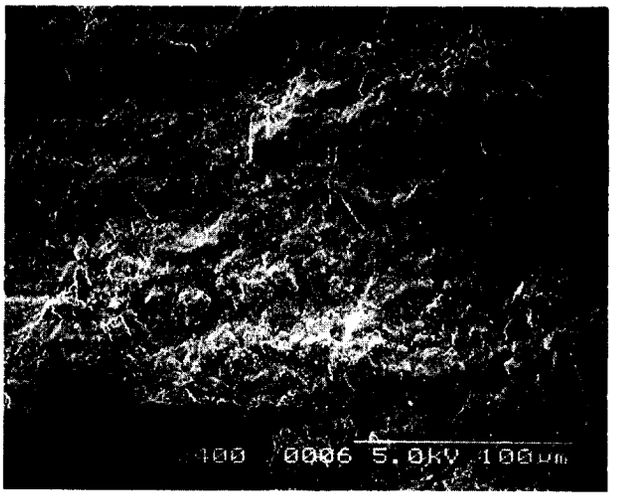

Fig. 5. Green microstructure of P1 powder pressed at 200 MPa, observed by SEM on fracture surface.

Fig. 6. Green microstructure of P3 powder pressed at 200 MPa, observed by SEM on fracture surface.

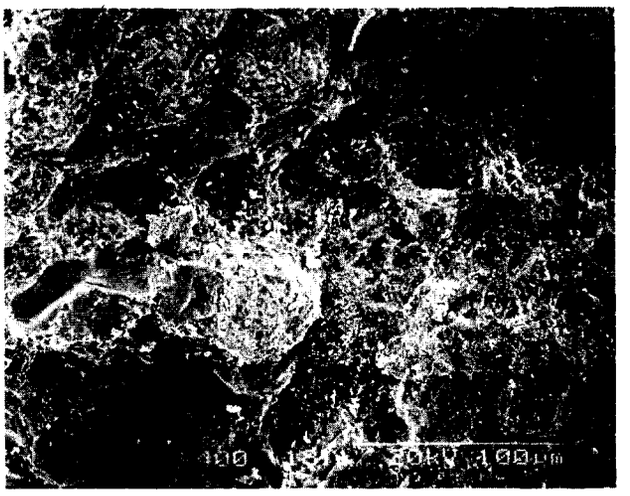

Fig. 8. Green microstructure of P2 powder pressed at 400 MPa, observed by SEM on fracture surface.

intercrystallite pores and intergranulate pores (these granulates are the starting powder granulates weakly deformed by the applied pressure). As pressure is increased, the later pore family is progressively diminished, but at 400 MPa the distribution still presents two maxima, corresponding to intercrystallite pores and intergranulate pores between the widely deformed granulates.

SEM observations substantiate the porosimetric results: at 200 MPa, in both P1 (Fig. 5) and P3 (Fig. 6) samples, the starting granulates lose their identity, although the presence of theses granulates is still well evident in the P2 sample (Fig. 7). At 400 MPa the initial granulates of the P2 powder are sufficiently deformed and the size of the largest intergranulate pores have been reduced but are still visible (Fig. 8).

Numerous relationships have been proposed to predict the tensile strength of monosized spherical particle packing.[17–21] On the basis of these relationships, it can be retained in a first approximation,

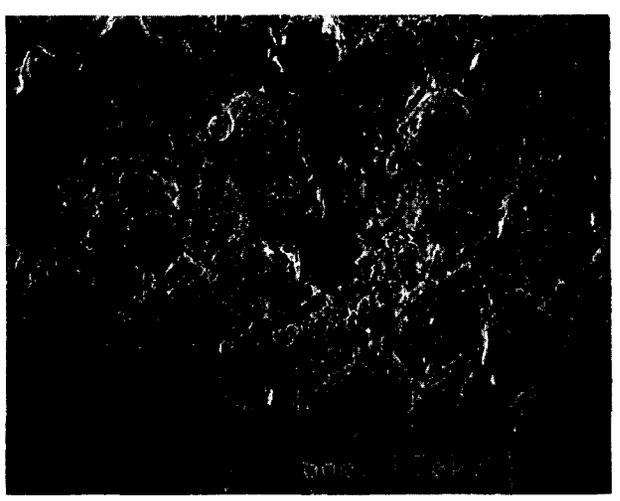

Fig. 7. Green microstructure of P2 powder pressed at 200 MPa, observed by SEM on fracture surface.

that the strength of a green body is related to the packing density, the particle diameter and the interparticle forces. It can be noticed that the JKR model,[20] elaborated on a brittle fracture base, takes also in account the defect size. Nevertheless the notion of defect in a granular material is difficult to define, especially in a granule, so this will not be taken into consideration here. Thus tensile strength is defined as the stress required to fracture a powder compact in simple tension, however these relationships remain useful to evaluate the resistance of a spherical granule under uniaxial compression.

In the case of the P1 powder, the intercrystalline binding generated during the synthesis is fully replaced by 'viscous' binding which depends on the nature of the polymer added. This permits a low breakpoint pressure and a visco-plastic behaviour, but requires some treatment of powder after synthesis.

The strength of P2 and P3 granules is only concerned with powder synthesis since no further treatment was conducted. As the crystallite sizes are the same, the two parameters that have to be considered to explain the difference in granule strength are the packing density and the nature of the intercrystallite forces. The packing density of the granules can be evaluated with consideration of the apparent density of the granules in the compacts. Galakchov[22] has proposed for slip cast green compacts, a method to obtain the apparent density of each powder unit, (aggregate, agglomerate,...), using the pore volume distribution. Indeed each peak of the pore volume distribution can be attributed to a powder unit, thus the apparent density of each unit can be calculated using the following expression:

$$\rho_{i+1} = \rho_i / 1 + \rho_i V_{i+1} \quad (1)$$

where ρ_i is the apparent density of the i^{th} order

unit, V_i is the specific volume of the pores contained in i^{th} unit in cm^3/g.

To obtain the granule density in compacted green samples, the applied pressure must be lower than the breakpoint pressure. This is, of course, to avoid any modification of intragranule porosity. With consideration of the compaction curves, compacts of P2 and P3 powders were obtained with pressures of 20 and 4 MPa respectively. Then Hg porosimetric measurements were conducted on these samples, but the intrusion pressure was limited to 280 MPa because of the fragmentation of the compacts with higher pressures. The pore volume distributions obtained at very low pressures (P < Py) shown a first peak located at large porosities. The pore volume of this peak can be connected with the intergranulate porosity. The pore channel sizes of this peak range from 0·04 to 4 μm for the P2 powder, and from 0·04 to 30 μm for the P3 powder. The first fraction of a second peak is observed, corresponding to intragranule porosities; the location of this peak is coherent with the pore distributions obtained with a compaction pressure of 100 MPa.

Two units in the powders are considered, the crystallites and the granules. Then from the previous expression, the two following expressions are used:

$$\text{apparent density of compacts: } d_o = \rho_g/1 + \rho_g V_{inter} \quad (2)$$

$$\text{first order units (granules) } \rho_g = \rho_o/1 + \rho_o V_{intra} \quad (3)$$

with V_{inter} and V_{intra} respectively the inter and intra-granules porosity. The tetragonal zirconia density (6·10 g/cm^3) was considered for the density of the crystallites ρ_0. The evaluation of the specific porosities (V_{inter} and V_{intra}) and the apparent densities of the granules and the compacts at the different compaction pressures are summarised in Table 2. In the case of low compaction pressures (P < Py), granule densities were obtained using expression (2) since V_{intra} was not measurable. From these calculations it appeared that the granule densities of the P2 and P3 powders were very close (2·168 and 2·095 g/cm^3 respectively). The granule densities are also given for high compaction pressures. Although the use of the term granule is arguable as P > Py, it can be seen from Table 2 that the reduction of intra-granule porosity with compaction pressure is more efficient in P3 granules. At P < Py, the more important inter-granule porosity of P3 compacts compares to P2, confirms that the lower tap density of P3 is due to inadequate granule sizes.

Consequently the granule strength appears to be essentially dependent on the intercrystallite forces induced during powder synthesis. Three kinds of bonds can be considered here: (i) Van der Waals, which concern all fine powders, (ii) solid bridge chemical bonds which may appear during a high temperature calcination step, because of initial sintering, and (iii) Zr–O–Zr chemicals bonds induced on drying after aqueous washing.[23] The Van der Waals bonds are weak and will lead to the formation of soft granules. On the other hand, the two others are strong. It has been extensively reported that hard granules are produced because of these bonds with direct sol–gel process. It can be assumed that solid bridge formation is avoided because of the low calcination temperatures used for powder synthesis. As a consequence of the difference in synthesis processes, we can suppose that Zr–O–Zr chemical bonds are more common in the P2 powder, and Van der Waals forces in the P3 powder.

Figure 9 displays the dilatometric results obtained from P1, P2 and P3 samples showing green densities of 55%, 47% and 49% TD, respectively. P2 and P3 samples exhibited lower starting sintering temperatures than that of sample P1 (1025°C for P1, 875°C for P2 and 950°C for P3): this is due to their smaller crystallite size and related higher reactivity. It can also be observed that the lower the green density, the higher the total shrinkage at 1500°C (18% for P1 <20% for P3 and <22·5% for P2). The high shrinkage may play a negative role in the industrial application of these powders, especially in the case of their utilisation in large and complex die designs.

A complete densification was achieved for the P1 sample at 1500°C and its microstructure was

Table 2. Specific pore volumes and apparent densities in P1 and P2 compacts obtained with different pressures

Compaction pressure (MPa)	*Intra-granules pore volume (cm^3/g)*		*Inter-granules pore volume (cm^3/g)*		*Granule apparent density (g/cm^3)*		*Compact apparent density (g/cm^3)*	
	P2	*P3*	*P2*	*P3*	*P2*	*P3*	*P2*	*P3*
$P < P_y$	—	—	0·181	0·575	2·168	2·095	1·557	0·951
100	0·230	0·257	0·135	0·020	2·540	2·377	1·891	2·267
200	0·243	0·209	0·061	0·010	2·456	2·678	1·137	2·607
400	0·142	0·123	0·014	0·008	3·270	3·481	1·131	3·381

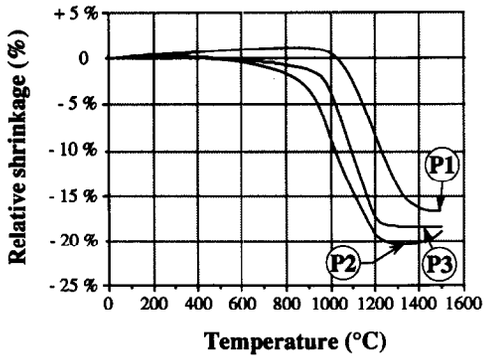

Fig. 9. Dilatometric curves of P1, P2 and P3 samples.

characterised by a uniform submicronic grain size (Fig. 10).

Above 1350°C a 'de-densification' step was observed on the dilatometric curve of the P2 sample. The same, but to a lesser extent, was also noticed on the P3 sample. This phenomenon, characterised by a more or less evident rise on the curves, may be ascribed to a secondary recrystallization, which leads to an abnormal grain growth[24-25] (Fig. 11). In addition, differential sintering phenomena are observed in the P2 sample, leading to circumferential cracks around residual granulates (Fig. 12). Then full densification is impeded by these large pore-like cracks.

So the dilatometric results can be well correlated to the green state: particle arrangements of poor quality in the green parts conducted to a shrinkage curve with a very low slope. In such a case, although the starting sintering temperature is low, the ending sintering temperature is very high because extensive grain growth must arise to allow further shrinkage, as soon as pores larger than the grains are present in the arrangement. At the extreme a total densification will not be possible since abnormal grain growth occurs before which residual porosities disappear by normal grain coarsening. Indeed during abnormal grain growth some pores will be trapped within grains before they have the opportunity to disappear and in noncubic crystalline structures a new class of pores can appear due to the fact that some grains can grow to sizes very much larger than the average particle size.

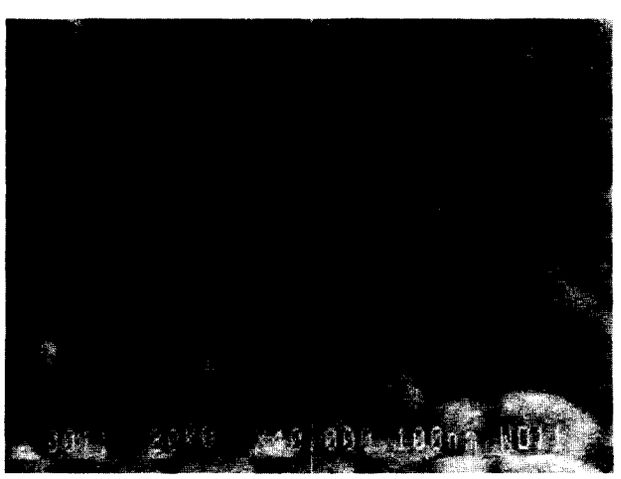

Fig. 10. Microstructure of P1 sample densified 2 h at 1500°C.

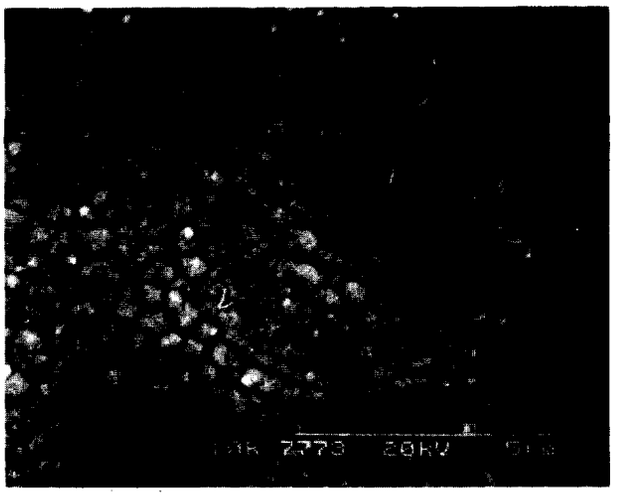

Fig. 11. Abnormal grain growth observed on P2 and P3 samples densified for 2 h at 1500°C.

To determine appropriate sintering conditions, powder pellets were heat treated at 1350°C and 1500°C. The final densities were evaluated and for each sample the relative density was determined on the ground of phase, (monoclinic and tetragonal) composition measured by X-ray diffraction analysis: Table 3 lists the results of XRD and density determinations.

Table 3. Dense material characteristics

Powder	*Sintering temperature (°C)*	*Monoclinic phase (%)*	*Apparent density (g/cm^3)*	*Density in % of theoretical*
P1	1350	0	6·05	99·1
	1500	0	6·05	99·1
P2	1350	0	5·92	97·1
	1500	0	5·35	97·7
P3	1350	42	5·85	99·8
	1500	74	5·62	98·8

Fig. 12. Circonferential cracks due to differential sintering of residual agglomerates observed on P2 densified sample.

For the P2 sample, the density values of the sintered bodies are in agreement with dilatometric curves, and confirm the 'de-densification' phenomenon observed at the higher temperatures. Up to a sintering temperature of 1350°C, no abnormal grain growth is observed in this material, and the grain size stays below 0·1 μm.

In the P3 sample, a density near the theoretical value is reached after sintering to 1350°C, although a high monoclinic zirconia content is present. At 1500°C, the monoclinic zirconia content is largely due to grain growth. This is ascribed to the low yttria content of the P3 powder (2 mol %). However, this is not the case for the P2 powder which contains 3·6 mol % of yttria. As a consequence the Y_2O_3 amount of the P3 powder is too low with respect to the microstructure to avoid the tetragonal–monoclinic transformation during cooling.

4 Conclusions

Each different synthesis process provides specific characteristics to the zirconia powder. The influence of these characteristics on application properties was studied. This allows us to evaluate the potential of sol–gel processes developed here. The significant parameters can be classified as:

— the fineness and reactivity of crystallites

— crystallite arrangement characteristics

— chemical composition

Concerning the first point, sol–gel processes usually allow a great improvement in reactivity. Consequently the starting sintering temperature is lowered.

Nevertheless crystallite size reduction is not a sufficient condition to achieve complete densification. To obtain an end sintering temperature very close to the starting sintering temperature, i.e. full densification at a low temperature, it is necessary to consider the second point and to realise parts with a green state of high quality. For fine powders it is well known that granulation is imperative. Sol–gel process offer many ways to obtain granulates. Two different methods have been tested here and can be summarised as follows:

Granulate sizes

The best results are obtained with large granules, typically 50–100 μm diameter. With minor changes to the process it will be possible to increase the granule diameters of the two sol–gel powders. Tap densities of the same order as the control powder P1 are expected.

Granulate morphology

To ensure good flowability of the powder and an easy reorganisation of the granules during compaction, a spherical geometry is needed. This condition is easily obtained with sol–gel processes. This is the case in the two methods studied here.

Granulate density

Sol–gel processes are able to produce better granules than the classic powders which are frequently spray dried: spray drying has the disadvantage of producing granulates with cavities, so that the tap density and the quality of the reorganisation during compaction are affected.

Granulate strength

The control of the granulate strength is the critical part of sol–gel processes, since industrial processes usually require compaction pressure under 100 MPa. The process used for P3 powder production allows us to produce low strength granules, by suppression of the detrimental chemical bonds Zr–O–Zr between crystallites. This results in compaction curves close to the control. But as it is not possible to use organic additives (a high temperature calcination is necessary after the granulation step), the production of sol–gel granules still encounter two major problems. Firstly, it is difficult to control the strength of the green parts, which is a major problem for industrial products. Secondly, the granule destruction arises by fragmentation instead of plastic deformation, and this is expected to be less efficient for porosity reduction. A process which solves these two problems, without any further treatment after granulation, have to be found, since this constitutes the major interest of sol–gel processes.

Chemical composition

The final point concerns the chemical composition of the powders. This point is of major importance since it has a great influence on the microstructure and phase composition of zirconia products. Sol–gel processes present the advantage of offering a better control of the chemical purity and homogeneity. For example, the stabilising agent distribution can be expected to be more homogeneous. But, as it can be seen with the P3 powder, the stabiliser amount must be optimised with respect to the final grain size.

Acknowledgement

The authors are grateful to CO.TR.A.O. (COmmunauté de TRavail des Alpes Occidentales) for their financial support of this research.

References

1. Zheng, J. & Reed, J. S., Effect of particle packing characteristics on solid state sintering. *J. Am. Ceram. Soc.*, **72**(5) (1989) 810–7.
2. Dynys, F. W. & Halloran J. W., Compaction of an aggregated powder. *J. Am. Ceram. Soc.*, **66**(9) (1983) 655–60.
3. Lange F. F., Sinterability of agglomerated powders. *J. Am. Ceram. Soc.*, **67**(2) (1984) 83–9.
4. Dynys, F. W. & Halloran, J. W., Influence of aggregates on sintering. *J. Am. Ceram. Soc.*, **67** (9) (1984) 596–601.
5. Matsumoto, R. L. K., Generation of powder compaction response diagrams. *J. Am. Ceram. Soc.*, **69**(10) (1986) C246–7.
6. Frey, R. G. & Halloran, J. W., Compaction behavior of spray-dried alumina. *J. Am. Ceram. Soc.*, **67**(3) (1984) 199–203.
7. Matsumoto, R. L. K., Analysis of powder compaction using a compaction rate diagram. *J. Am. Ceram. Soc.*, **73**(2) (1990) 465–8.
8. Niesz, D. E. & Bennett, R. B., Structure and properties of agglomerates. In *Ceramic processing before firing*, ed. G. Y. Onoda & L. L. Hench, Wiley Interscience Publication, 1978, pp. 61–73.
9. Hench, L. L. & Ulrich, D. R., Ultrastructure processing of ceramics, glasses and composites, J. Wiley, New York, 1984.
10. Readey, M. J., Lee, R. R., Halloran, J. W. & Heuer, A. H., Processing and sintering of ultrafine MgO–ZrO_2 and (MgO,Y_2O_3)–ZrO_2 powders, *J. Am. Ceram. Soc.*, **73** (6) (1990) 1499–503.
11. Montanaro, L., Elaboration des poudres ceramiques par voie sol–gel: application au dispersoïde alumine–zircone et à la zircone yttriée. PhD thesis, I.N.P.G. — ENS des Mines de St. Etienne, 1990.
12. Garvie, R. C. & Nicholson, P. S., Phase analysis in zirconia systems. *J. Am. Ceram. Soc.*, **55**(6) (1972) 303–5.
13. Alexander, L. E. & Klugt, H. P., *X-ray diffraction procedures for polycrystalline and amorphous materials*. John Wiley & Sons Ed., New York, 1974.
14. AFNOR French normalization, *Powder metallurgy — determination of tap density*. NF A 95-112 (equivalent to ISO 3953-1977).
15. Vergnon, P., Sur la compressibilité des poudres. *Rev. Int. Hautes Températures et Réfract*, **3** (1966) 399–408.
16. Bortzmeyer, D., Compaction des poudres céramiques. PhD Thesis, E. N. S. des Mines de Paris, 1990.
17. Rumpf, H., *Chem. Intgr. Tech.*, **42** (1970), 538–40.
18. Schubert, H, Tensile strength of agglomerates. *Powder Technol.*, **11** (1975) 107–19.
19. Cheng, D. C. H., *Chem. Eng. Sci.*, **23** (1968) 1405.
20. Johnson, K. L., Kendall, K. & Roberts, A. D., *Proc. Royal Soc. London*, (1961), A324, 301.
21. Thompson, R. A., *Ceram. Bull.*, **60**(2) (1981) 248–51.
22. Galakchov, A. V. & Shevchenko, V. J., Influence of pore structure inhomogeneities in green compacts on strength and reliability of Y-TZP, *J. Europ. Ceram. Soc.*, **6** (1990) 317–22.
23. Kaliszewski, M. S. & Hever, A. H., Alcohol interaction with zirconia powders. *J. Am. Ceram. Soc.*, **73** (1990) 1504–9.
24. Kingery, W. D., *Ceramic fabrication processes*, John Wiley & Sons Ed., New York, 1958.
25. Coble, R. L., *Sintering and related phenomena*. Gordon & Breach Ed., New York, 1967.